Varying-Time Random Effects Models for Longitudinal Data: Unmixing and Temporal Interpolation of Remote Sensing Data

Hervé CARDOT[(1)], Philippe MAISONGRANDE[(2)] and Robert FAIVRE[(3)]
(1) Université de Bourgogne, Institut de Mathématiques, UMR CNRS 5584,
9, avenue Alain Savary - B.P. 47 870, 21078 Dijon, France
(2) Centre D'Etudes Spatiales de la Biosphère, UMR CNES-CNRS,
18 Av. Edouard Belin, 31401 Toulouse, France.
(3) INRA Toulouse, Unité Biométrie et Intelligence Artificielle,
31326 Castanet-Tolosan, Cedex, France.

December 14, 2006

Abstract

Remote sensing is an helpful tool for crop monitoring or vegetation growth estimation at a country or regional scale. However, satellite images generally have to cope with a compromise between the time frequency of observations and their resolution (*i.e.* pixel size). When concerned with high temporal resolution, we have to work with information on the basis of kilometric pixels, named mixed pixels, that represent aggregated responses of multiple land cover. Disaggreggation or unmixing is then necessary to downscale from the square kilometer to the local dynamic of each theme (crop, wood, meadows,...).

Assuming the land use is known, that is to say the proportion of each theme within each mixed pixel, we propose to address the downscaling issue through the generalization of varying-time regression models for longitudinal data and/or functional data by introducing random individual effects. The estimators are built by expanding the mixed pixels trajectories with B-splines functions and maximizing the log-likelihood with a Backfitting-ECME algorithm. A BLUP formula allows then to get the "best possible" estimations of the local temporal responses of each crop when observing mixed pixels trajectories. We show that this model has many potential applications in remote sensing and an interesting one consists in coupling high and low spatial resolution images in order to perform temporal interpolation of high spatial resolution images (20m), increasing the knowledge on particular crops in very precise locations.

The unmixing and temporal high resolution interpolation approaches are illustrated on remote sensing data obtained on the South-Western of France during the year 2002.

keywords: Backfitting, BLUP, covariance function, downscaling, ECME, functional data, mixed effects, mixed pixels, splines, SPOT/VGT, SPOT/HRVIR, remote sensing

1 Introduction

Satellites are increasingly used in many domains of the earth sciences such as oceanography, meteorology or continental surfaces studies (see for example Richards & Jia, 2005 or the web sites `http://www.noaa.gov/eos.html` and `http://www.eumetsat.int/`). For continental surfaces, vegetation and more specifically crops can be observed and studied with optical remote sensing. These observations consist in reflectances, which are ratios between reflected and incoming energy, principally at two wavelengths (Red: 0.6μm and Near InfraRed: 0.9 μm) according to the spectral signature of green leaves (Richardson & Wiegang 1977, Knipling 1970). Thanks to these properties, reflectances and their combinations are able to reveal the impact of pedoclimatic conditions or agriculture practices on the vegetation and crops dynamic.

At the scale of crop fields, reflectances provided by satellite optical sensors permit to estimate models parameters and dynamic variables (Moulin *et al.* 1995, Moulin *et al.* 1998, Ridao *et al.* 1998, Kastens *et al.* 2005). The interest of such data of course lies in the time and geographic dimension that are the specific advantages of satellite imagery.

However, the earth observation from space has to cope with a dilemma between repetitiveness and pixels resolution. Nowadays, quasi daily global coverage are available for free at kilometric (NOAA/AVHRR missions) and sub-kilometric resolution (250m) with for example the MODIS or MERIS missions. On the other hand, the observation at 20 meters (or less) that would be necessary for crop applications can hardly be delivered more often than once per month for small regional scales and at expensive prices. The time frequency of low resolution data would be satisfying in case the pixel heterogeneity can be overcame. Disaggregation or unmixing (Faivre & Fischer, 1997, Lobell *et al.* 2004) is then necessary to downscale from the square kilometer to the local dynamic of each vegetation type (crop, wood, meadows,...).

In this context, our study is devoted to the presentation and evaluation of an original statistical methodology for the unmixing issue which takes advantage of the high time frequency of low resolution data in order to increase the repetitiveness of high resolution time series.

The spatial aggregation problem is described in Figure (1) which presents the same area observed both with sensors at high and low spatial resolutions. For example, in the visible and the near infra-red wavelengths, onboard the two last spot satellites SPOT 4 and SPOT 5, a daily global coverage of

continental surfaces is made possible at kilometric resolution thanks to the VEGETATION sensor (Maisongrande *et al.* 2004). On the same platform, the HRVIR (High Resolution) sensor provides users with regional scenes (60km×60km) at 20m resolution but its repetitiveness of observation on a specific region reaches hardly one available image per month (Coret *et al.* 2005). This means that frequent images are only made available on the basis of kilometric pixels that represent aggregated responses of multiple land cover inside each low resolution pixel. Figure (1) shows that aggregation induces a non negligible amount of loss of spatial information and, as a consequence, a loss of precision on the crop development in each plot. The unmixing problem consists in recovering the local trajectories knowing the noisy aggregated response and the proportions of land surface of the different themes within a mixed pixel. We may expect to get accurate enough estimations of these local behavior by taking into account the *temporal evolution* of the aggregated trajectories.

We address this downscaling issue on the basis of a natural statistical model relying on mixed effects for longitudinal data (Laird & Ware, 1982). This model is a direct extension to longitudinal (Diggle *et al.* 1994) and functional data (Rice 2004, Ramsay & Silverman, 2005) of a previous work by Faivre & Fischer (1997) who considered the downscaling problem for only one image, that is to say at one date, and thus without taking into account the temporal structure of the correlation. Our approach allows to take implicitly into account the spatial and temporal variations of the different responses without having to assume explicitly any kind of spatial correlation that would lead to nearly intractable estimation procedures.

Although parametric growth models exist for some specific crops, they are not available for most of the themes under studies. Furthermore, these parametric models are nonlinear and the existing estimation procedures for nonlinear mixed effects models are nowadays still not efficient enough to cope with such large data sets (see *e.g* Déjean *et al.* 2002). Let us also remark that interesting hierarchical bayesian approaches (Wikle *et al.* 2001) have also been proposed in such spatiotemporal contexts. They lead to rather heavy estimating procedures and rely on reasonable *a priori* for the temporal covariance structure. There are no natural parametric candidate for the *a priori* in our context.

Our approach is different and we propose a statistical nonparametric model which appears to be rather simple and well adapted to deal with very large data sets. We propose to expand the temporal trajectories with B-splines functions which are known to provide both accurate approximations to smooth functions (Dierckx, 1993), which is a natural assumption for phenological curves, and a parsimonious nonparametric model. It is a direct extension of the model studied by Hoover *et al.* (1998) who did not introduce random effects in their varying-time regression model. Once the

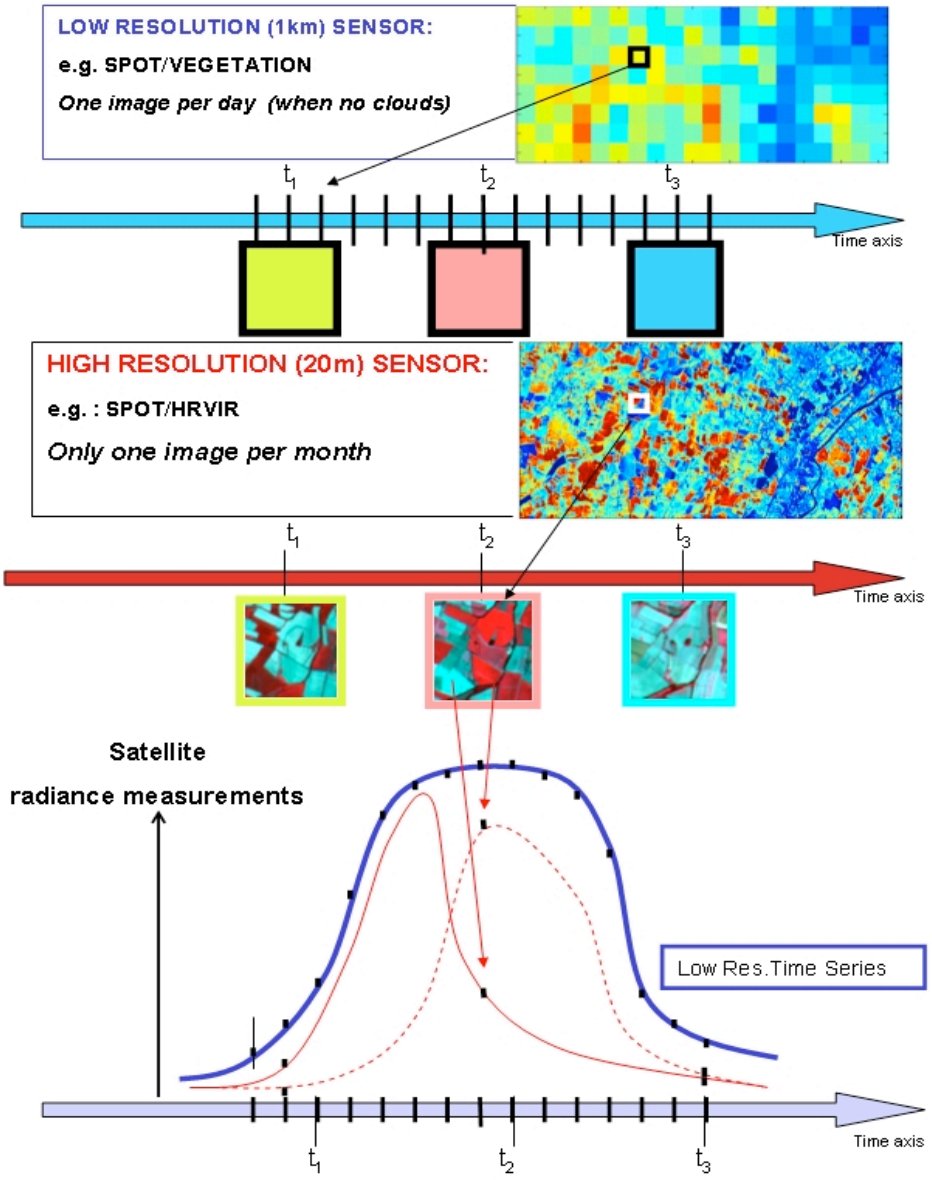

Figure 1: With satellite images, technical constraints oblige to choose between repetitiveness and pixels resolution. We present, along time, a same scene observed at two different resolution and repetitiveness. On top, the temporal evolution observed by the Low Resolution Sensor SPOT4/VGT at many frequent dates (potentially 1 image per day). The bottom part shows sparse time series of three high resolution images acquired by SPOT4/HRVIR (hardly available once per month). The blue bold line represents the time profile for a heterogeneous low resolution pixel while the 2 thin red curves stand for the 2 inner elementary land cover types and their respective time trajectory (that can only be measured at too sparse time frequency by high resolution sensors). Length of the time axis is about one year.

parameters, mean curves and covariance functions of the different themes, are estimated, unmixing is performed using a BLUP formula to get the best approximation of the individual responses. The BLUP formula also allows us to perform temporal interpolation of high resolution remote sensing data when observing both low resolution with a high time frequency and high resolution images at a few different dates (between 3 and 10). Our estimation procedure relies on maximizing the log-likelihood function according to the coordinates in the B-splines basis by combining a weighted backfitting procedure (Hastie & Tibshirani, 1990) for the fixed effects and an ECME step (Mac Lachlan & Krishnan, 1997) for the variance components. Our model can also be interpreted as a generalization of the functional PCA for mixtures of curves when the mixture coefficients, *i.e.* the proportions of land use of each theme within mixed pixels, are known. The proposed algorithm is rather effective and it takes only a few minutes to converge with images representing area of about 4500 km^2 with 35 dates of observation and a land use classification composed of 7 different themes. Let us note that a similar varying time regression model with random effects has been proposed by Wu & Liang (2004). Nevertheless, their estimator, which is based on local polynomials, does not seem to be suitable for such large remote sensing datasets since it only considers the univariate case and extending their approach to multivariate covariates is not immediate at all.

In section 2, we present the aggregation model and give an empirical justification for such a mixed effects approach based on functional principal components analysis (Ramsay & Silverman, 2005) of some high resolution trajectories. Section 3 describes the estimation procedure. In section 4 a brief simulation study confirms the good properties of the B-splines approximation and the optimization algorithm. Section 5 presents a real life application in the South-Western France, a region for which we have, during year 2002, a sequence of 36 medium resolution VEGETATION images as well as 10 SPOT4/HRVIR high resolution images inside an area of about 4500 km^2. Finally, section 6 proposes a general discussion, some extensions of this approach and what could be next investigations.

2 The aggregation model of phenological curves

Before going on, let us fix some notations. We suppose we have p low spatial resolution images observed at p different instants during the season, $t_1 < t_2 < \cdots < t_p$, which are not necessarily equi-spaced. Each image is composed of n coarse resolution pixels i, $i = 1, \ldots, n$ and for each pixel i we get a discretized trajectory $\mathbf{X}_i = (X_i(t_1), \ldots, X_i(t_p))' \in \mathbb{R}^p$ where $\mathbf{X}_i$ is either the observed reflectance curve for a certain channel (BLUE, RED, GREEN or NIR) or for a Vegetation Index which is a linear combination of the reflectance for different channels. We also suppose that the land use is

known, that is to say we have the proportion π_{ij} of surface of each theme j, $j = 1, \ldots, J$ within each pixel i. They satisfy $\pi_{ij} \geq 0$ and $\sum_{j=1}^{J} \pi_{ij} = 1$.

In the visible and the near infra-red wavelengths, a natural aggregation model (Foody & Cox, 1994) of the responses of the different themes is the following one:

$$X_i(t) = \sum_{j=1}^{J} \pi_{ij} \ \rho_{ij}(t) + \varepsilon_{i,t}, \quad t \in \{t_1, t_2, \cdots, t_p\}, \tag{1}$$

where $\rho_{ij}(t)$ is the reflectance curve, or "phenological curve" for theme j (*e.g.* crop type), within pixel i and the noises $\varepsilon_{i,t}$ are supposed to be independent and drawn from a Gaussian distribution with mean zero and variance σ^2. Let us notice that model (1) can not infer generally directly at the parcel scale since there can be many different parcels of a same crop within a coarse resolution pixel. Our model only describes the "mean" response $\rho_{ij}(t)$ of plots of crop j within pixel i, that is to say the mean responses of the different parcels of a same crop. Nevertheless, it is generally well adapted for modeling local responses of crops since the intra-pixel (or within pixel) variabilities are relatively small compared to the inter or between (mixed) pixel variabilities. This hypothesis is realistic for remote sensing when dealing with pixels whose size is about 1km^2. Indeed, within such a surface, the assumption of "homogeneity" in the responses of different plots of a same crop is often satisfied.

Unfortunately the parameters of interest $\rho_{ij}(t)$ of model (1) can not be identified when observing the aggregated responses $X_i(t)$. To cope with this problem, Cardot *et al.* (2003) made following simplification

$$\rho_{ij}(t) = \rho_j(t), \quad t \in [0, T], \tag{2}$$

assuming that, for relatively small areas (around 40 km $\times$ 40km), the response of a culture does not vary with the location i of the pixel. One major drawback of this approach is that it does not take into account the local variations of the phenological curves assuming the growth of a culture as being nearly identical in all the considered area. Unfortunately this might not be the case (see next section), even for regions with moderate size, since factors such as soil composition or climate may also vary spatially, influencing locally the crop development and its temporal evolution. Thus, one has to find an intermediate model between the overparametrized model (1) and the too simple model (2).

2.1 Towards a mixed effects approach

Thanks to a regional scientific project involving the high resolution monitoring of a specific region near Toulouse ("Sud-Ouest" project, see section

5 for more details), we also have a time series of 10 dates of high resolution images (SPOT4/HRVIR) during year 2002. This dataset allows the diagnostic of variations of the responses of each vegetation type around its mean phenological curve.

For instance, let us have a closer look at temporal responses according to the PVI index (Tucker, 1979) of pixels composed only of "wheat crops" (see Figure 2). The PVI index, a linear combination of the responses in the RED and NIR channels defined by PVI=a NIR- b RED with $a = 0.62$ and $b = 0.78$ in this region, shows that assumption (2) is really too strong. One cannot assume that variations of the "wheat" pixel trajectories around its mean phenological curve are only due to independent noises as supposed in (2). Indeed a functional PCA (Ramsay & Silverman, 2005), which can also be interpreted as a mixed effects model (Rice & Wu 2001), exhibits a high temporal correlation structure, meaning that the variations around the mean function $\rho_j(t)$ have a strong temporal structure and projecting the data onto a 2-dimensional space of functions allows to explain more than 70 % of the whole variability.

Looking now at the two last displays in Figure (2), in which we have drawn the densities of the principal components, one clearly sees that even if the principal components are not exactly Gaussian they are clearly unimodal and can be approximated, at first sight, without much error, by Gaussian random variables. Having in mind these consideration Cardot *et al.* (2004) proposed a Gaussian mixed effects model in order to describe the temporal behavior of mixed pixels.

Assuming the response of the different themes are independent and that the temporal correlation of the themes does not depend on the location, we propose the following model

$$\left\{ \begin{array}{rcl} X_i(t) & = & \displaystyle\sum_{j=1}^{J} \pi_{ij}\ \rho_{ij}(t) + \varepsilon_{i,t}, \quad t \in \{t_1, \ldots, t_p\}, \\ \boldsymbol{\rho}_{ij} & \sim & \mathcal{N}\left(\boldsymbol{\rho}_j, \boldsymbol{\Gamma}_j\right), \quad j = 1, \ldots, J, \end{array} \right. \tag{3}$$

where $\rho_j(t)$ is the expectation of the random function $\rho_{ij}(t)$, $\boldsymbol{\rho}_j = (\rho_j(t_1), \ldots, \rho_j(t_p))'$, $\boldsymbol{\rho}_{ij} = (\rho_{ij}(t_1), \ldots, \rho_{ij}(t_p))'$ and $\boldsymbol{\Gamma}_j = \mathbb{E}\left(\boldsymbol{\rho}_{ij} - \boldsymbol{\rho}_j\right)\left(\boldsymbol{\rho}_{ij} - \boldsymbol{\rho}_j\right)'$ is the covariance matrix with elements

$$[\boldsymbol{\Gamma}_j]_{\ell,\ell'} = \mathrm{Cov}(\rho_{ij}(t_\ell), \rho_{ij}(t_{\ell'})) = \gamma_j(t_\ell, t_{\ell'}), \quad \ell, \ell' = 1, \ldots p.$$

The noise components $\varepsilon_{i,t}$ are supposed to be independent and Gaussian with mean zero and variance σ^2. Model (3) is a random effects varying-time regression model.

2.2 Interpolation and prediction with the BLUP formula

Unmixing and temporal interpolation can be handled naturally with the BLUP formula (Robinson, 1991) which is recalled now. If $(\mathbf{U}, \mathbf{V})$ is a Gaus-

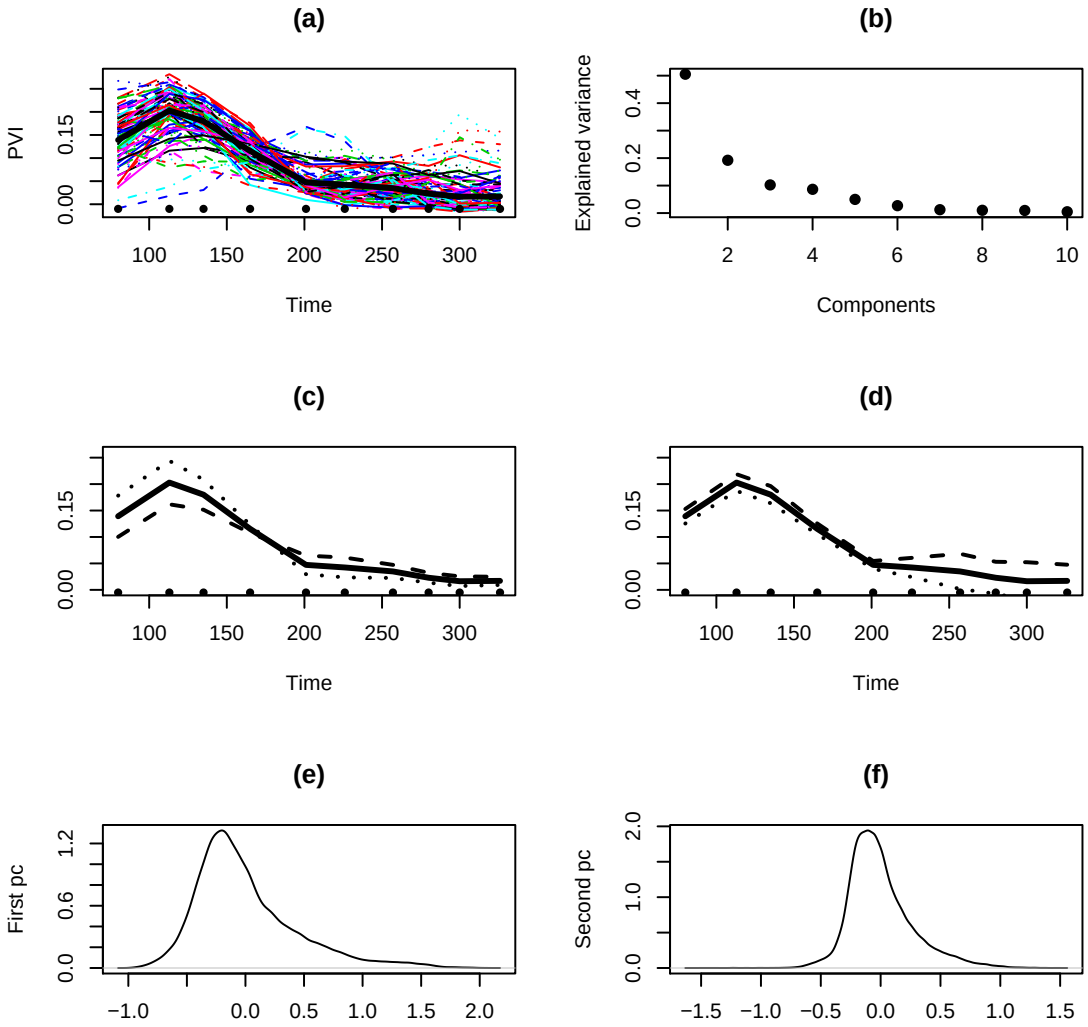

Figure 2: Functional Principal Components Analysis of the response of the PVI of high resolution pixels observed at 10 different instants during year 2002 and containing 100 % of the theme "Wheat". The graphs represent a/ a sample of one hundred wheat pixels trajectories, b/ the explained variance by the ten principal components, c/ and d/ the variation around the mean trajectories induced by respectively the first and second eigenfunctions, e/ and f/ the density of the first and second principal components.

sian multivariate random variable

$$(\mathbf{U}, \mathbf{V}) \sim N\left(\begin{pmatrix} \boldsymbol{\mu}_u \\ \boldsymbol{\mu}_v \end{pmatrix}, \begin{pmatrix} \boldsymbol{\Gamma}_u & \boldsymbol{\Gamma}_{u,v} \\ \boldsymbol{\Gamma}_{v,u} & \boldsymbol{\Gamma}_v \end{pmatrix}\right)$$

the best linear unbiased prediction of the component $\mathbf{U}$ having observed $\mathbf{V} = \mathbf{v}$, is given by the well known BLUP formula

$$\mathbb{E}\left(\mathbf{U}|\mathbf{V} = \mathbf{v}\right) = \boldsymbol{\mu}_u + \boldsymbol{\Gamma}_{u,v}\boldsymbol{\Gamma}_v^{-1}\left(\mathbf{v} - \boldsymbol{\mu}_v\right) \ . \tag{4}$$

Going back to our study and assuming that $X_i, \pi_{ij}, \boldsymbol{\rho}_j$, $\boldsymbol{\Gamma}_j$ and σ^2 are known, we can give an answer to the first question, that is to say determine the best estimation of the response of a crop within a mixed pixel. Taking $U = \rho_{ij}(t)$ and $\mathbf{V} = \mathbf{X}_i = (X_i(t_1), \ldots, X_i(t_p))'$ we get

$$\mathbb{E}\left(\rho_{ij}(t) \mid \mathbf{X}_i\right) \ = \ \rho_j(t) + \mathrm{Cov}(\rho_{ij}(t), \mathbf{X}_i)\left[\mathrm{Var}(\mathbf{X}_i)\right]^{-1}\left(\mathbf{X}_i - \sum_{j=1}^{J}\pi_{ij}\boldsymbol{\rho}_j(t)\right) \tag{5}$$

where

$$\mathrm{Cov}(\rho_{ij}(t), \mathbf{X}_i) = \pi_{ij}\left(\gamma_j(t, t_1), \ldots, \gamma_j(t, t_p)\right)$$

and

$$\left[\mathrm{Var}(\mathbf{X}_i)\right]_{\ell,\ell'} = \sigma^2 I_{\{\ell=\ell'\}} + \sum_{j=1}^{J}\pi_{ij}^2\gamma_j(t_\ell, t_{\ell'}) \ .$$

Suppose we now observe a plot with a higher resolution sensor at a few instants $\tau_1, \ldots, \tau_\kappa$ with $\kappa << p$. We assume each pixel of this sensor is pure, that is to say its underlying surface is only occupied by one crop, and as before we suppose the variability of the response of each crop is very small for crops located in the same mixed pixel. If these assumtions are satisfied, which is the case in practice (see discussion in the concluding remarks) then temporal trajectory of the high resolution pixel can be estimated (using the best linear predictor) at any other instant τ. Assuming that we also observe during the same period of time (but not necessarily the same instants) the trajectory of the underlying mixed pixel $\mathbf{X}_i = \left(X_i(t_1), \ldots, X_i(t_p)\right)$, temporal interpolation is performed by applying the BLUP formula (4) with $U = \rho_{ij}(\tau)$ and $\mathbf{V} = \mathbf{V}_i = (\rho_{ij}(\tau_1), \ldots, \rho_{ij}(\tau_\kappa), X_i(t_1), \ldots, X_i(t_p))' \in \mathbf{R}^{\kappa+p}$. Then

$$\mathbb{E}\rho_{ij}(\tau) \ = \ \rho_j(\tau) + \mathrm{Cov}(\rho_{ij}(\tau), \mathbf{V}_i)\left[\mathrm{Var}(\mathbf{V}_i)\right]^{-1}\left(\mathbf{V}_i - \mathbb{E}\mathbf{V}_i\right)$$

with $\mathbb{E}\mathbf{V}_i = \left(\rho_j(\tau_1), \ldots, \rho_j(\tau_\kappa), \sum_{j=1}^{J}\pi_{ij}\rho_j(t_1), \ldots, \sum_{j=1}^{J}\pi_{ij}\rho_j(t_p)\right)'$.

Note that we can also get the conditional variance both for the interpolation and disaggregation approaches.

3 Maximum likelihood estimators

We first propose to expand the observed aggregated trajectories with B-splines basis. Then we can get an approximation to the likelihood function and look for its maximum with an algorithm that combines Backfitting for the fixed effects and ECME for the random components.

3.1 B-Splines approximation of the phenological curves and their conditional variances

Trajectories are expanded in B-splines basis (Dierckx, 1993) in order to have a finite and relatively small number of parameters to estimate. These functions are known to provide parsimonious and good approximations to "smooth functions" such as the true phenological curves. Thanks to their local support, they also have good numerical properties, which is not the case for polynomial approximation. To gain in flexibility, we consider two different basis for the mean phenological curves and for the individual variations. We take a B-splines basis, $B_1(t), \ldots, B_{K_1}(t)$, (resp. $\mathcal{B}_1(t), \ldots, \mathcal{B}_{K_2}(t)$) of order q_1 (resp. q_2) with k_1 (resp. k_2) equi-spaced interior knots in the period of interest for the expansion of the mean phenological curves (resp. the individual variations) where $K_1 = k_1 + q_1$ (resp. $K_2 = k_2 + q_2$) is the dimension of the functional space spanned by the B-splines.

Approximation to the individual responses can be written as follows

$$\rho_{ij}(t) \approx \sum_{k=1}^{K_1} \theta_{k,j} B_k(t) + \sum_{s=1}^{K_2} \delta_{s,j}^i \mathcal{B}_s(t), \tag{6}$$

separating the fixed effects, $\theta_{k,j}$, from the random effects $\delta_{s,j}^i$ which are supposed to be centered. Going back to the mixed pixels trajectories, we get the formulation for the aggregated data

$$X_i(t_\nu) \approx \sum_{j=1}^{J} \pi_{ij} \sum_{k=1}^{K_1} \theta_{k,j} B_k(t_\nu) + \sum_{j=1}^{J} \pi_{ij} \sum_{s=1}^{K_2} \delta_{s,j}^i \mathcal{B}_s(t_\nu) + \varepsilon_{i,t_\nu}, \tag{7}$$

for $\nu = 1, \ldots, p$ and $i = 1, \ldots, n$. Denoting by $\gamma_j^{s,\ell} = \mathrm{Cov}(\delta_{s,j}^i, \delta_{\ell,j}^i)$, this can also be written in a matrix way as follows

$$\mathbb{E}(\mathbf{X}_i) = \mathbf{B}\boldsymbol{\theta}\boldsymbol{\pi}_i \tag{8}$$

$$\mathrm{Var}(\mathbf{X}_i) = \sigma^2 \mathbf{I}_p + \sum_{j=1}^{J} \pi_{ij}^2 \sum_{s,\ell=1}^{K_2} \gamma_j^{s,\ell} \boldsymbol{\mathcal{B}}_s \boldsymbol{\mathcal{B}}_\ell' \tag{9}$$

where $\mathbf{X}_i = (X_i(t_1), \ldots, X_i(t_p))$, $\boldsymbol{\theta}$ is the matrix $K_1 \times J$ whose elements are $[\boldsymbol{\theta}]_{k,j} = \theta_{k,j}$, $\mathbf{B}$ is the matrix $p \times K_1$ whose elements are $[\mathbf{B}]_{\nu,k} = B_k(t_\nu)$, $\mathbf{B}_k = (B_k(t_1), \ldots, B_k(t_p))'$ and $\boldsymbol{\mathcal{B}}_s = (\mathcal{B}_s(t_1), \ldots, \mathcal{B}_s(t_p))'$.

Remark 1 *Note that (9) does not assume that $\delta^i_{s,j}$ and $\delta^i_{s',j}$ are independent for $s \neq s'$ but we assume that there is no correlation between different themes. As a matter of fact, it is easily seen that one can get estimations of the cross covariance function since this assumption is not required in the estimation procedure (see below), at the expense however of a much larger number of parameters to be estimated. We focus here on crop trajectories and not on the relation between crops and this is the main reason why this assumption was made since .*

Remark 2 *Such a B-splines decomposition is still valid even if the pixels are not exactly observed at the same instants which is the case for instance when we have S10 synthesis (see e.g. Duchemin & Maisongrande 2002, Maisongrande et al. 2004). With S10 synthesis, the image is composed of pixels whose value is the best response in term of measurement quality (no clouds, no aerosol, ...) among ten consecutive days. To remain valid, we only have to assume that there is at least one time measurement between two adjacent interior knots which is generally true if the number of knots is not too high. Then, one can consider vectors $\mathbf{B}_{k,i}$ and $\boldsymbol{\mathcal{B}}_{s,i}$ that depend on i without modifying the estimation procedure described below.*

3.2 The likelihood function

At this stage, let us introduce the following notation. Denote by $\mathbf{V}_i$ the $p \times p$ variance matrix of the digitized trajectory $\mathbf{X}_i$, defined in (9),

$$\mathbf{V}_i \quad = \quad \sigma^2 \mathbf{I}_p + \sum_{j=1}^{J} \pi_{ij}^2 \boldsymbol{\mathcal{B}} \tilde{\boldsymbol{\Gamma}}_j \boldsymbol{\mathcal{B}}' \tag{10}$$

where $\boldsymbol{\mathcal{B}}$ is the $p \times K_2$ matrix with generic element $[\boldsymbol{\mathcal{B}}]_{\nu,k} = \mathcal{B}_k(t_\nu)$ and $\tilde{\boldsymbol{\Gamma}}_j$ is a matrix $K_2 \times K_2$ whose elements are $[\tilde{\boldsymbol{\Gamma}}_j]_{s,l} = \gamma_j^{s,l}$.

The log-likelihood, equals, up to a constant,

$$\mathcal{L} = -\frac{1}{2}\left(\sum_{i=1}^{n} \log|\mathbf{V}_i| + \sum_{i=1}^{n} (\mathbf{X}_i - \mathbf{B}\boldsymbol{\theta}\boldsymbol{\pi}_i)' \mathbf{V}_i^{-1} (\mathbf{X}_i - \mathbf{B}\boldsymbol{\theta}\boldsymbol{\pi}_i)\right) \tag{11}$$

and the parameters to be estimated are σ^2, the $K_1 \times J$ matrix $\boldsymbol{\theta}$ and the J covariance matrices $\tilde{\boldsymbol{\Gamma}}_j$ whose sizes are $K_2 \times K_2$.

3.3 The optimization algorithm

The estimation procedure proposed here is based on combination of the backfitting algorithm and a kind of EM algorithm (Laird & Ware, 1982), called ECME which is known to converge faster than the classical EM algorithm (McLachlan & Krishnan, 1997). Let us note that one major advantage

of this approach compared to direct optimization procedures is that the estimated covariance matrices are automatically non negative.

One reasonable approach to maximize (11) is to consider an alternating procedure for linear mixed models and conditional variance estimation. The steps of the algorithm are the following ones

1. Initialization: get $\widehat{\boldsymbol{\theta}}^0$ by classical least squares (see Cardot *et. al.*, 2003).
2. Determine an estimator of the variance components $\tilde{\boldsymbol{\Gamma}}_j$ and σ^2 with the ECME step (see below).
3. Maximize the likelihood according to $\boldsymbol{\theta}$, $\widehat{\tilde{\boldsymbol{\Gamma}}_{\boldsymbol{j}}}$ and $\widehat{\sigma}^2$ being obtained at previous step. This step is equivalent to a weighted least squares minimization.
4. Iterate steps 2 and 3 until convergence. The algorithm is stopped when the variations of $\widehat{\sigma}^2$ are less than 0.001.

Once the algorithm has converged, we can deduce estimation of the phenological curves for each instant t,

$$\widehat{\rho}_j(t) = \sum_{k=1}^{K_1} \widehat{\theta}_{k,j} B_k(t) \tag{12}$$

as well as the covariance functions

$$\widehat{\gamma}_j(s,t) = \boldsymbol{\mathcal{B}}'(s)\widehat{\tilde{\boldsymbol{\Gamma}}_{\boldsymbol{j}}}\boldsymbol{\mathcal{B}}(t) \tag{13}$$

where $\boldsymbol{\mathcal{B}}(t) = (\mathcal{B}_1(t), \ldots, \mathcal{B}_{K_2}(t))'$.

These steps are described in details in the following sections.

3.3.1 Estimating the variance components with ECME

Let us denote by $\boldsymbol{\delta}_j^i = (\delta_{1,j}^i, \ldots, \delta_{K_2,j}^i)'$ the vector individual components.

Assuming that we have estimators (obtained during previous iteration of the algorithm) for the individual covariance matrices, $\widehat{\mathbf{V}}_i$, we can deduce the conditional expectations for the individual components $\widehat{\boldsymbol{\delta}}_j^i = \mathbb{E}\left(\boldsymbol{\delta}_j^i \mid \mathbf{X}_i\right)$ as well as $\widehat{\boldsymbol{\varepsilon}}_i = \mathbb{E}\left(\boldsymbol{\varepsilon}_i \mid \mathbf{X}_i\right)$ using the BLUP formula,

$$\widehat{\boldsymbol{\delta}}_j^i = \pi_{ij}\tilde{\boldsymbol{\Gamma}}_j\boldsymbol{\mathcal{B}}'\widehat{\mathbf{V}}_i^{-1}\left(\mathbf{X}_i - \sum_{j=1}^{J}\pi_{ij}\mathbf{B}\widehat{\boldsymbol{\theta}}_j\right), \tag{14}$$

$$\widehat{\boldsymbol{\varepsilon}}_i = \mathbf{Y}_i - \sum_{j=1}^{J}\pi_{ij}\left(\mathbf{B}\widehat{\boldsymbol{\theta}}_j + \boldsymbol{\mathcal{B}}\widehat{\boldsymbol{\delta}}_j^i\right). \tag{15}$$

With these expressions we can get estimates of the variance components

$$\begin{aligned} n\,\widehat{\widetilde{\mathbf{\Gamma}}}_j &= \mathbb{E}\left(\sum_{i=1}^{n}\widehat{\boldsymbol{\delta}}_j^i(\widehat{\boldsymbol{\delta}}_j^i)' \mid \mathbf{X}_i\right) \\ &= \sum_{i=1}^{n}\left\{\widehat{\boldsymbol{\delta}}_j^i(\widehat{\boldsymbol{\delta}}_j^i)' + \mathrm{Var}\left(\boldsymbol{\delta}_j^i \mid \mathbf{X}_i\right)\right\}. \end{aligned} \tag{16}$$

The variance σ^2 of the noise is estimated by

$$\begin{aligned} np\,\widehat{\sigma}^2 &= \mathbb{E}\left(\sum_{i=1}^{n}\boldsymbol{\varepsilon}_i'\boldsymbol{\varepsilon}_i \mid \mathbf{X}_i, \widehat{\widetilde{\mathbf{\Gamma}}}_1, \ldots, \widehat{\widetilde{\mathbf{\Gamma}}}_p\right) \\ &= \sum_{i=1}^{n}\left\{\widehat{\boldsymbol{\varepsilon}}_i'\widehat{\boldsymbol{\varepsilon}}_i + \mathrm{tr}\ \mathrm{Var}\left(\boldsymbol{\varepsilon}_i \mid \mathbf{X}_i\right)\right\}. \end{aligned} \tag{17}$$

Formulas for the expected conditional variances are given in McLachlan & Krishnan (1997).

3.3.2 A backfitting algorithm for weighted least squares iterations

Let us notice that the least squares criterion corresponding to step 0 and step 3 in the previous algorithm can also be expressed in a matrix way as follows :

$$\min_{\boldsymbol{\theta}}\ \varphi(\boldsymbol{\theta}) = \sum_{i=1}^{n}\left\|\mathbf{X}_i - \sum_{j=1}^{J}\pi_{ij}\mathbf{B}\widehat{\boldsymbol{\theta}}_j\right\|^2_{\mathbf{V}_i^{-1}}, \tag{18}$$

where $\|\mathbf{X}\|^2_{\mathbf{V}_i^{-1}} = \mathbf{X}'\mathbf{V}_i^{-1}\mathbf{X}$. Then, finding the roots of the set of score equations

$$\left.\frac{\partial\varphi(\boldsymbol{\theta})}{\partial\boldsymbol{\theta}_j}\right|_{\boldsymbol{\theta}=\widehat{\boldsymbol{\theta}}} = \mathbf{0}, \quad j = 1, \ldots, J, \tag{19}$$

is equivalent to solve the problem according to $\boldsymbol{\theta}_1, \ldots, \boldsymbol{\theta}_J$

$$\sum_{j'=1}^{J}\left(\sum_{i=1}^{n}\pi_{ij}\pi_{ij'}\mathbf{B}'\mathbf{V}_i^{-1}\mathbf{B}\right)\boldsymbol{\theta}_{j'} = \sum_{i=1}^{n}\pi_{ij}\mathbf{B}'\mathbf{V}_i^{-1}\mathbf{X}_i, \quad j = 1, \ldots, J. \tag{20}$$

Solving this system of equations can be done rather rapidly by blocks with the backfitting algorithm (Hastie & Tibshirani, 1990).

4 A simulation study

Before applying our method to real datasets we perform a brief simulation study in order to evaluate the effectiveness of the estimation procedure.

We have simulated $n = 1000$ aggregated trajectories

$$X_i(t) = \sum_{j=1}^{J} \pi_{ij}\ \rho_{ij}(t) + \epsilon_{i,t}$$

with

- $i = 1, \ldots, n = 1000$ pixels
- $p = 40$ instants sorted in ascending order, $t_1 \leq \ldots \leq t_p$, and drawn from a Uniform distribution in $[0, 1]$.
- $\mathrm{Var}(\epsilon_{i,t}) = \sigma^2 = 0.05$
- Land use : $j = 1, \ldots, J = 3$ classes and the π_{ij} are drawn from an uniform law in $[0, 1]$ and then normalized as follows $\pi_{i1} + \pi_{i2} + \pi_{i3} = 1$
- The high resolution trajectories are gaussian processes with mean and covariance functions evaluated for t and s belonging to $\{t_1, \ldots, t_p\}$:
  $\rho_1(t) = 5\exp(-(t-0.5)^2/0.1), \quad \gamma_1(s,t) = \exp(-|s-t|)$,
  $\rho_2(t) = 6\exp(-(t-0.4)^2/0.02), \quad \gamma_2(s,t) = (1+4(t-s)^2)^{-2}$
  $\rho_3(t) = 6\exp(-(t-0.7)^2/0.05), \quad \gamma_3(s,t) = (1+4(t-s)^2)^{-4}$

The mean response curves ρ_1, ρ_2 and ρ_3 can be understood as classical phenological curves (not scaled in this simulation study) with a growing period and then a decreasing one. They differ each other from the growing rates and the instants they reach their maximum.

In the estimation procedure, we have chosen $k_1 = k_2 = 5$ interior knots and order $q_1 = q_2 = 3$ so that $K_1 = K_2 = 8$ for the B-splines functions, allowing for a certain flexibility without needing to estimate too many parameters. We also consider other basis, allowing the number of interior knots to vary: it appeared, provided this number is not too low (not less than 4 to avoid larger bias) and not too high (not more than 10 to avoid increasing variance), the results are quite the same. The algorithm, coded in R, is fast and takes less than one minute to converge with $1 + 3 \times 8 + 3 \times 8 \times 9/2 = 133$ estimated parameters.

Unmixing aggregated trajectories

We have drawn in Figure 3 a realization of X and the estimated mean response curves defined in (12). We clearly see that the B-splines expansion give very accurate estimations to the mean behavior of the different themes. If we study the variance components, the conclusion are quite the same. The estimator $\widehat{\sigma}^2 = 0.048$ whereas the true value is 0.05. Considering now the loss criterion

$$\frac{\sum_{\ell,\ell'}^{p} \left(\widehat{\gamma}_j(t_\ell, t_{\ell'}) - \gamma_j(t_\ell, t_{\ell'})\right)^2}{\sum_{\ell,\ell'}^{p} \gamma_j(t_\ell, t_{\ell'})^2}$$

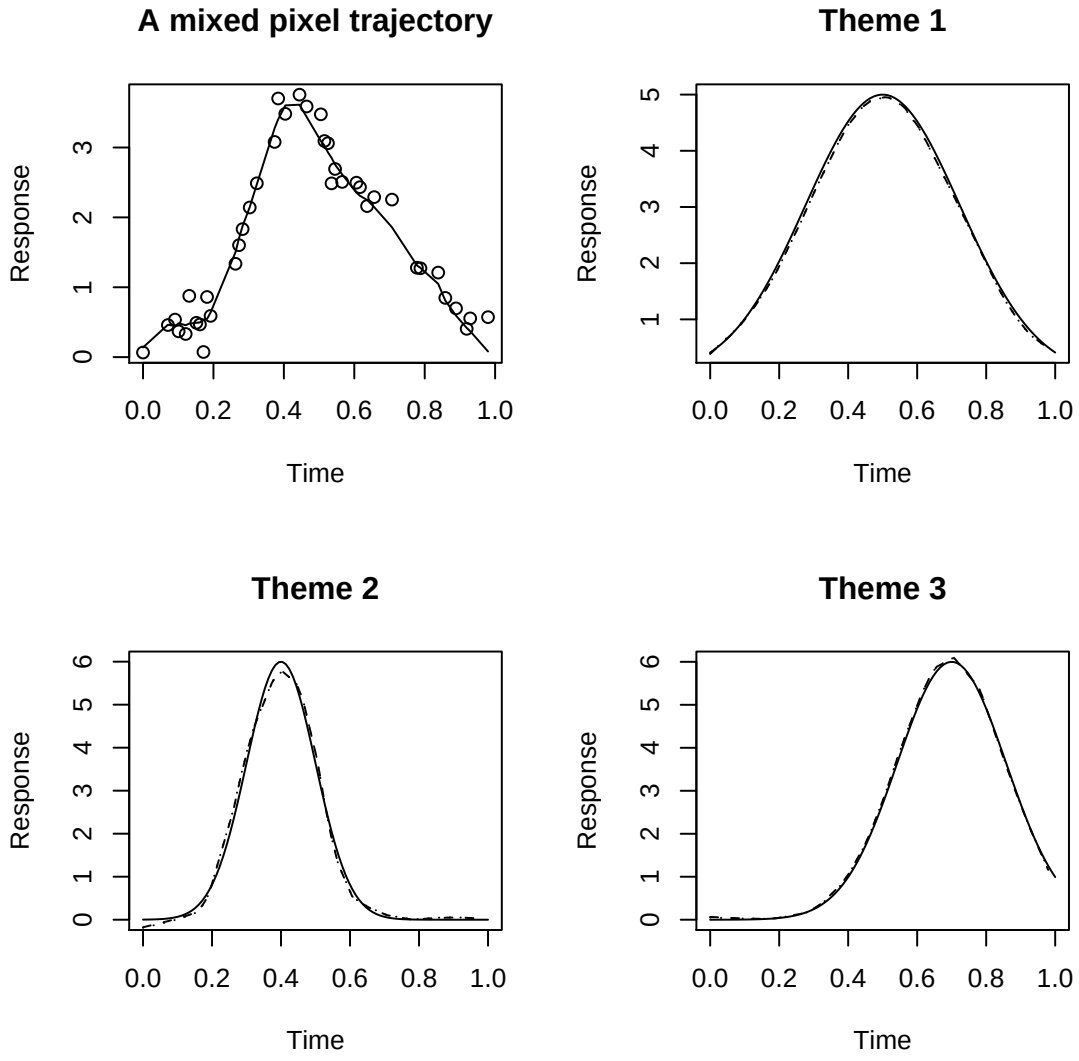

Figure 3: An example of simulated mixed pixel trajectory (plain line) and its noisy discretized observation (circles). True (plain line) and estimated (dotted line) mean response curves of the three different classes.

to evaluate the skill of the covariance term estimation, we get an error of about 0.06 for $\widehat{\gamma}_1$, 0.04 for $\widehat{\gamma}_2$, and 0.08 for $\widehat{\gamma}_3$, which means that we have obtained rather good approximations to the true covariance functions.

Let us look now, in Figure 4, at the estimation of the local responses, $\widehat{\rho}_{ij}$ obtained thanks to the BLUP formula. We first notice that if the proportion of the theme (theme 3 here with $\pi_{i3} = 0.49$) is sufficiently high, then there is an important gain in considering a mixed effects model and our estimators are able to capture rather well the variations from the mean response curve. On the other hand, if the proportion of the theme is not high enough (theme 1, with $\pi_{i3} = 0.23$), that is to say its contribution to the aggregated curve X_i is too low, then the individual curves is very similar to the mean response of the theme and there is no real gain in considering a mixed effects model for estimating individual trajectories.

Temporal interpolation of high resolution trajectories

To study the sensitivity of the quality of interpolation to the number ℓ of high resolution points, we consider a number ℓ of observed high resolution images varying from $\ell = 3$ to $\ell = 9$, the ℓ instants being equispaced in $[0, 1]$.

We compare 4 interpolation approaches, ordered according to an increasing level of information, and thus with increasing theoretical performances

- performing a linear interpolation of the high resolution trajectories ("lin" interpolation method).
- taking into account the estimated mean response curve and performing a linear interpolation of the local variation (the residuals) around this mean trajectory. This corresponds to a BLUP interpolation with a predefined covariance function ("res" interpolation method).
- applying the BLUP formula (4) which takes into account both the mean phenological curve and the covariance function. It gives the linear optimal interpolation of a stochastic process with known mean and covariance function. Theses functions are estimated in practice with our algorithm. ("blup1" interpolation method).
- taking into account both the high resolution and the low resolution trajectories in the BLUP formula ("blup2" interpolation method).

The difference between "blup1" and "blup2" is that the latter also take into account the trajectory of the low resolution underlying pixel to get the conditional expectation, thanks to the BLUP formula, of the high resolution response.

The error is evaluated with the mean square error of approximation at the predicted points. Table 1 gives these errors when interpolating trajecto-

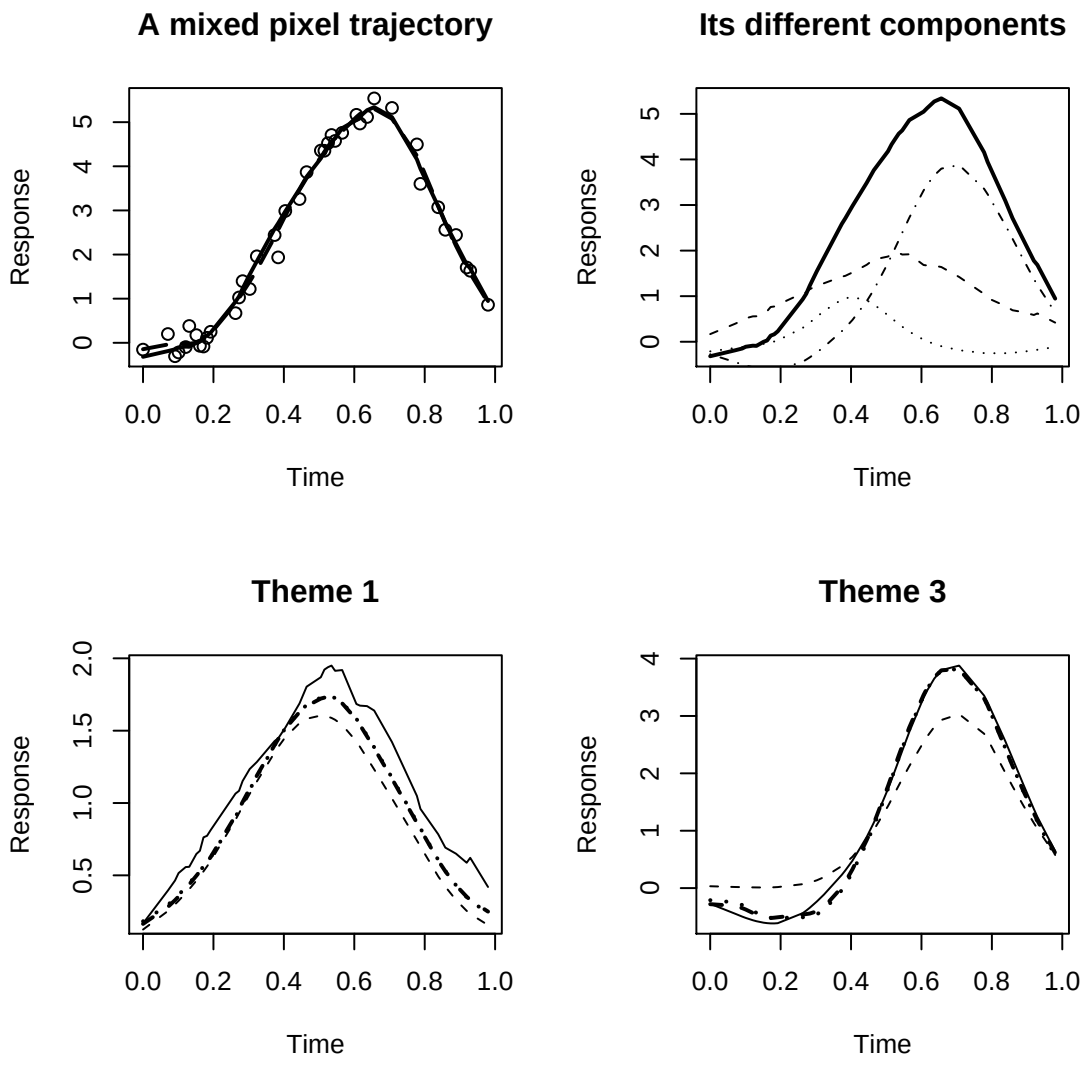

Figure 4: An example of simulated mixed pixel trajectory (bold line) and its noisy discretized observation (circles). The second display presents the true trajectory (bold line) as well as the contribution of the three different themes (dotted lines). The third and fourth displays present the contribution of the first and third theme (line), whose corresponding proportions are $\pi_{i1} = 0.23$ and $\pi_{i3} = 0.49$, the estimated weighted mean response of the theme (dotted line) and the estimated individual component (bold dotted line).

MSE	3 pts	5 pts	7 pts	9 pts
lin	2.65	0.57	0.26	0.038
res	0.24	0.081	0.051	0.011
blup1	0.23	0.052	0.022	0.004
blup2	0.12	0.037	0.018	0.004

Table 1: Mean Square Error (MSE) of interpolation according to the number of observed high resolution data for the four different approaches.

MSE	3 pts	5 pts	7 pts	9 pts
lin	2.65	0.56	0.26	0.038
res	0.25	0.082	0.052	0.011
blup1	0.24	0.052	0.021	0.004
blup2	0.051	0.024	0.014	0.004

Table 2: Mean Square Error (MSE) of interpolation according to the number of observed high resolution data for the four different approaches when considering mixed pixels containing more than 40 % of theme 3.

ries of crops belonging to theme 3. We first remark that the linear interpolation is not effective at all when the number ℓ of measurements is too low. The "res" method does not perform too badly, the information brought by the mean phenological curve telling what are the most important variations of the crop. Nevertheless, as the temporal information increases, the two blup approaches get better and better, allowing to take into account smaller variations. The blup2 approach is always better and provides good interpolations even for a small number of high spatial resolution data. Finally, when $\ell = 9$, the two blup approaches give similar errors, meaning that coarse resolution data do not bring additional information anymore.

If we restrict now the computation of the loss criterion to the pixels containing more than 40 % of theme 3, we can see in Table (2) that the information brought by the aggregated trajectories still improve significantly the prediction error made by the blup2 method, even for a small number ℓ of high resolution data.

5 Application: the "Sud-Ouest" project

In this section, the synthetic exercise previously described is now applied to an actual remote sensing dataset. Thanks to the "Sud-Ouest" Project (`http://www.cesbio.ups-tlse.fr/us/sud_ouest.html`) carried on at CESBIO, we took advantage of the simultaneous availability of high and low resolution

	Forest	Wheat	Maize	Pastures
1st axis	42 %	67 %	49 %	63 %
2nd axis	23 %	22 %	24 %	21 %
3rd axis	15 %	6 %	12 %	11 %

Table 3: Explained variance by the first three eigenfunctions of the estimated covariance operators of four important "crops" in the South-Western project.

time series during year 2002. Indeed, we have at our disposal 36 VEGETATION images, *i.e.* one image every 10 days (S10 synthesis see Maisongrande *et al.* 2004) as well as 10 high resolution images SPOT4/HRV (Coret et al. 2005). Within this pilot site, we have selected an area with a surface of about n =4500 km^2 in the South-Western of France. We consider the $J = 7$ most important themes in this region, which are Forest 9%, Wheat 22%, Maize 8%, Sunflower 12%, Pastures 26%, Urban 12% and "Remaining" representing 11 % of the total surface. The land use classification was made at CESBIO (Ducrot *et al.* 2004) using a classification algorithm based on multi-spectral and multi-temporal high resolution data.

5.1 Unmixing VEGETATION data

We first calibrate, with the land use and the VEGETATION data, the random effects model to get estimates of the mean temporal profiles of the different themes (equation 12) as well as their covariance functions (equation 13) using the algorithm described previously. The estimated mean phenological curves of the themes "Forest", "Wheat", "Maize" and "Pastures" are drawn in Figure (5) where we can clearly see that the responses along time of the different types of vegetation vary in their intensities but also in their variabilities. For instance, the theme "Pastures" seems to have larger variations, from one location to another, than other crops. To study in details the largest mode of variations of these classes, we have derived the eigenelements of the estimated covariance functions. The variance explained by the first three principal components are given in Table 3. We can notice that mainly all the variability of these crops, that is to say more than 80 % of the total variations, is captured by approximating the individual trajectories in a two dimensional space for "Wheat" and "Pastures" and a three dimensional space for the themes "Forest" and "Maize".

We have also drawn in Figure (6) the first two eigenfunctions for these crops. This also clearly points out that the principal modes of variability can be very different from one crop to another. This also tends to improve the ability of the BLUP formula to discriminate between the contributions of the different crops inside a mixed pixel.

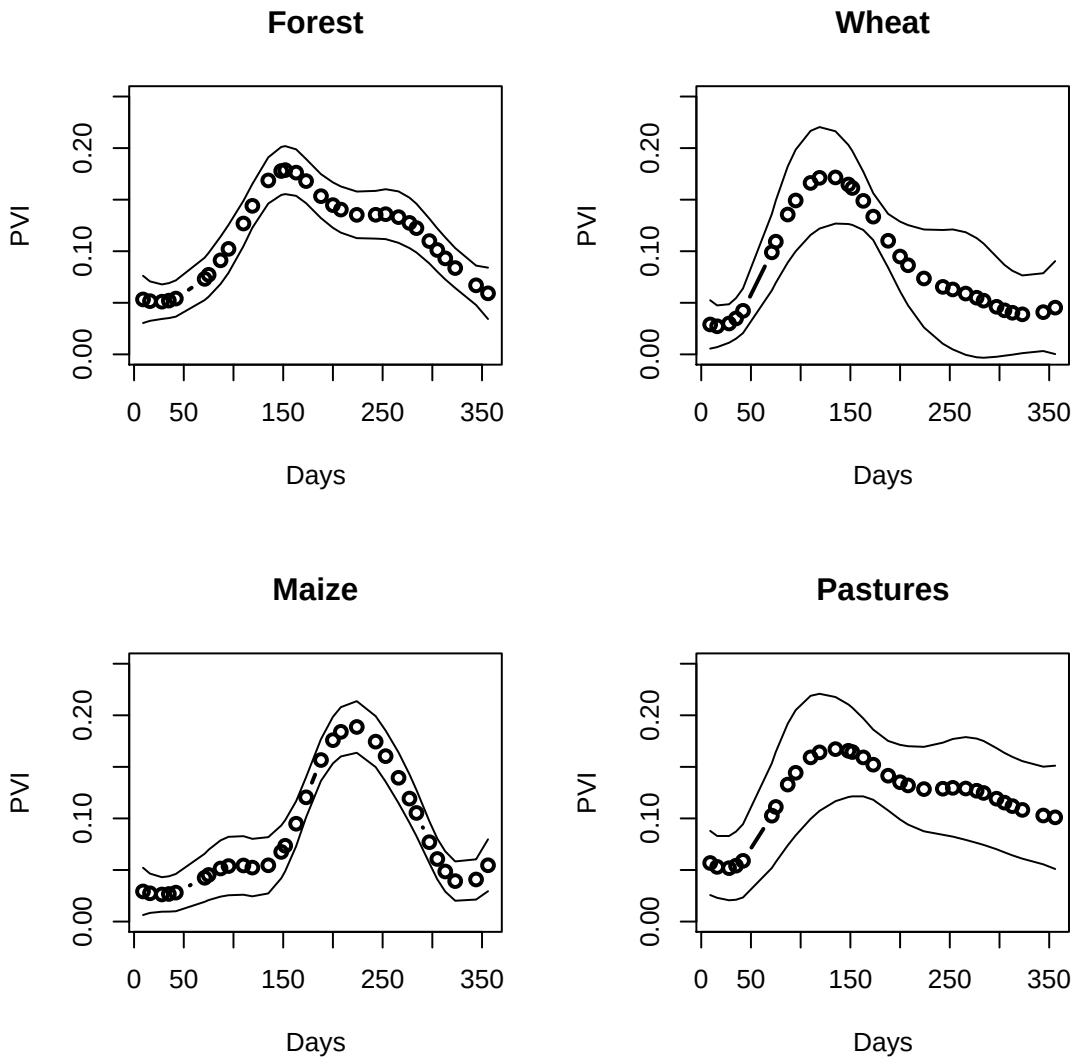

Figure 5: Estimated mean phenological curves (circles) with the PVI during year 2002 with VEGETATION data for the themes "Forest", "Wheat", "Maize" and "Pastures". We have added ± two times the instantaneous standard deviations in order to characterize the main instants in time of variability (plain lines).

MSE	All pixels	Surf $\geq$40%
lin	6.64	4.68
res	4.68	2.85
blup1	4.78	2.08
blup2	4.09	2.05

Table 4: Interpolation errors of the PVI index for the SPOT4 high resolution pixels containing "Wheat" crops as well as those for which the "Wheat" plots represent more than 40 % of the total surface.

Note that phenologies presented in Figure (5) are in very good agreement with expected time behaviours for "Forest", "Wheat", "Maize" and "Pastures" classes that have already been investigated by Coret *et al.* (2005) on the basis high resolution time series. The mean phenology for forest is quite realistic, its maximum occurs in May (*i.e.* slightly later than winter crops and grass), and, similarly to "Wheat" and "Pasture", it decreases from late spring to September because of the water stress occurring in the Midi Pyrénées Region. Automnal re-growth due to new rain fall can be seen as well on every class but "Maize".

"Wheat" and "Pastures" show quasi-equivalent time phasing in winter and early spring. Their time pattern get slightly different at "Wheat" senescence prior to the harvest, when pasture also get dry but often keep a higher greenness. The phenology of "Maize" that we estimate is perfectly realistic as well. Its fast increase of leaves from May to August is due to the irrigation, prior to the senescence phase.

It is also realistic to observe lower intraclass time variability for "Forest" and "Maize" than for "Wheat and "Pastures". Due to its roots depth, Forest presents a lower sensitivity to the summer water depletion in the upper soil than wheat and pasture do. The explanation for the low dispersion for Maize is the regional homogeneity of cultural practices in term of sowing calendar and irrigation practices.

5.2 Temporal interpolation of SPOT4/HRVIR data

In the same area, high resolution images were available at a few number of time instants, $\tau_1 < \ldots < \tau_{10}$. In order to evaluate the ability of the mixed effects approach to get approximations to high resolution trajectories, we have supposed that we have observed only 4 High Resolution images (at the dates $\tau_1, \tau_3, \tau_5, \tau_8$) and we want to estimate the evolution for the 6 other dates. The mean square errors of prediction, with the PVI index for the theme "Wheat", are presented in Table 4.

We first notice that taking into account VEGETATION data (medium

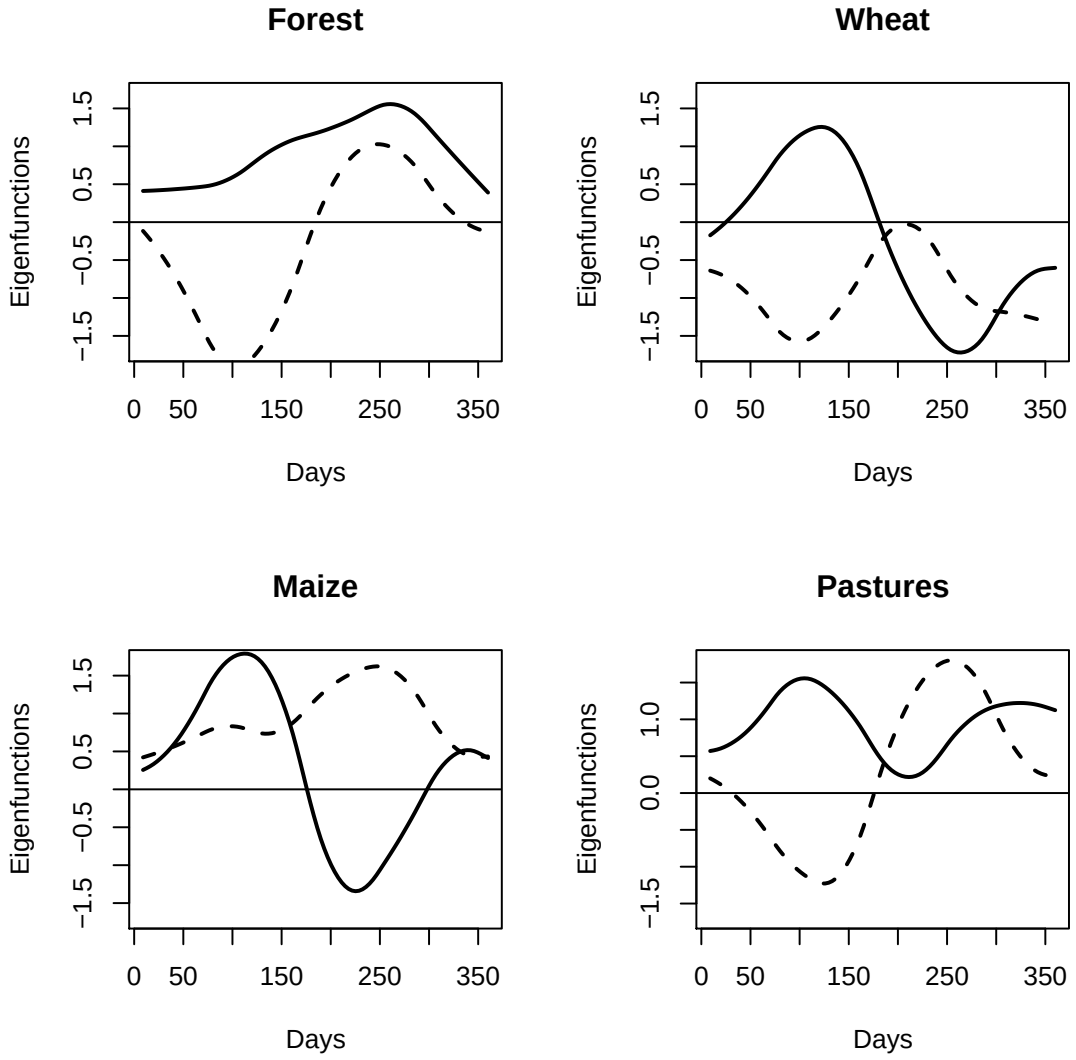

Figure 6: Estimated first two eigenfunctions during year 2002 with VEGETATION data for the themes "Forest", "Wheat", "Maize" and "Pastures". The first eigenfunction is drawn in plain lines whereas the second one is in dotted lines.

resolution trajectories) allows us to get better temporal interpolation of high resolution data. Indeed, the "lin" method performs poorly compared to the approaches incorporating VEGETATION data. The gain can be rather important, the error being divided by two compared to the "lin" method, when considering pixels containing more 40 % of wheat crops. Nevertheless, even if the methods based on the BLUP give better predictions, the main improvement in the interpolation seems to be due to the knowledge of the mean temporal response in the area under study.

Many factors can explain this lack of improvement and the main one seems to be a *calibration problem*, meaning that the reflectances of the two different sensors are not exactly calibrated the same way and thus the temporal evolution of medium resolution pixels is not as useful as it could be for interpolating high resolution ones. This is clearly seen in Figure 7 where we have drawn the mean phenological curves of four different crops according to the two spatial resolutions for the PVI index.

6 Concluding remarks

Downscaling reflectances of mixed pixels is an important but difficult issue in remote sensing, allowing to deduce with physical models many useful local information such as water demand, soil moisture, crops development or to derive finer land use classifications. Unfortunately, when using satellite data, one often has to cope with a compromise between resolution and time frequency. The low resolution imagery is cheap and frequent but its drawback is the aggregative character of the radiometric information it contains.

The simulation study clearly shows that taking into account simultaneously the information brought by sensors with different resolutions can lead to considerable potential gain in temporal interpolation of High Resolution data. Nevertheless, our work also points out the need for an as good as possible HR layer versus LR layer juxtaposition when one wants to take advantage of the complementarity between the two types of data. The required consistency principally depends on various factors such as: sensors inter-calibration, accuracy of each layer georeferencing, projections consistency, and also neighborhood effects (between adjacent pixels) which present patterns that are resolution dependent. Although a particular attention was paid on these different points, residual artifacts (principally geometric) might persist and explain a part of the difference between the synthetic and the real data exercise. This issue is beyond the scope of the paper but deserves further attention. For example, we logically expect a gain of consistency when reducing the resolution gap when considering 250 m resolution data (*e.g.* MODIS sensor) instead of the kilometric pixels of SPOT/VEGETATION. This statistical approach can also be helpful to address the combination of Low and High Resolution (information brought

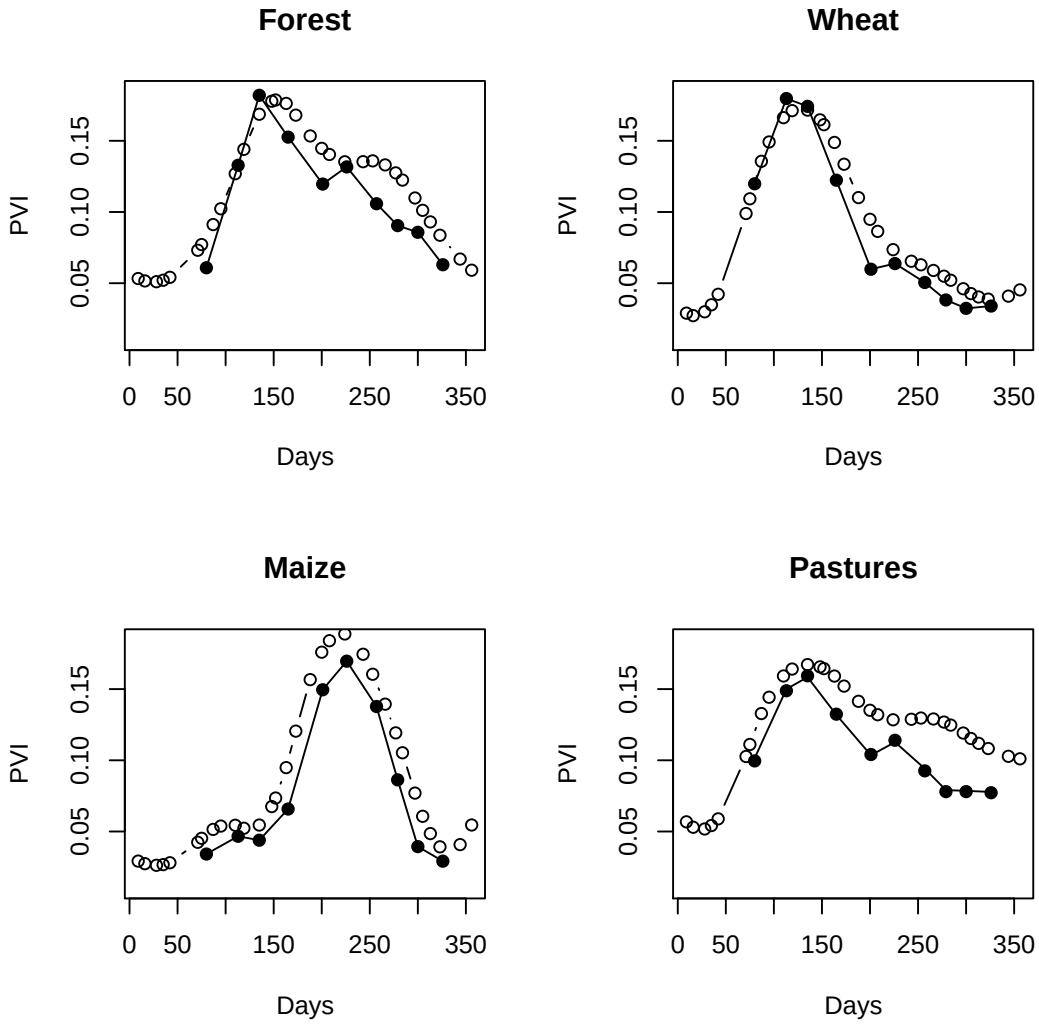

Figure 7: Comparison of the estimations of phenological curves according to the resolution of the sensor, small circles for SPOT4/VEGETATION, lines with black points for SPOT4/HRVIR.

by both types of sensors) making thus possible studies necessary to the dimensioning of future satellite missions that could combine the two types of sensors. Space Agencies and satellite makers could for example evaluate the number and type of sensors that will have to operate simultaneously in order to ensure a sufficiently frequent crop monitoring, at a specified level of precision.

Besides remote sensing considerations, another point of interest is the determination of the domain of validity of such an aggregation model when there are spatial correlations between the temporal responses of a particular crop. The ideal case for the model to be valid is when there is no variation within a mixed pixel, meaning that all the variations of the responses of different crops are between mixed pixel variations. On the contrary, the worst case would be when all the variability is concentrated within coarse resolution pixels, meaning that we have a kind of "fractal" property. If we assume that the spatial correlation is very large for very close neighbors and low for far ones, which is a realistic assumption for crops, we can suppose that we are not too far from the ideal case. Nevertheless this needs to be quantified and deserves further investigations. Then, one interesting question is what would be the best spatial resolution for disaggregation when observing mixed pixels and thus how sensors should be calibrated ?

Another interesting issue is the extension to nonlinear indices such as the $NDVI$ index which is a non-linear combination of the responses in the RED and Near Infra Red (Tucker, 1979). This index is widely used in the remote sensing community because it can give a good measure of the state of a crop and it has certain robustness properties. In order to get local estimation of this index, one has to extend our random effect model and consider a multivariate response disaggregation model, with outputs $RED(t)$ and $NIR(t)$, and then perform a Taylor expansion of this index. Applying the BLUP formula to this linear approximation allows to get local estimations of the $NDVI$. We are working on this topic but this is beyond the scope of this paper.

More generally, the proposed approach for disaggregation is based on mixed effects models for longitudinal data and is able to handle huge samples with many time measurements. Mixed effects models are widely used in other contexts such as medicine, biology (Diggle *et al.* 1994) and economy (Wooldridge, 2002) allowing to describe individual characteristics with random parameters statistical models but generally with a low number of individuals or a low number of measurements. Nowadays it is frequent to have longitudinal data with both many individuals and many time measurements. Our nonparametric approach which can also incorporate effectively the effects of a relatively large number of covariates seems to be a good candidate for such studies. The proposed nonparametric methodology is rather

efficient, leading to accurate estimation with a fast algorithm as shown in the simulation study.

Acknowledgments: We would like to thank all the participants to the working group "Changement d'échelle" in Toulouse for fruitful discussions. We would like to thank G. Dedieu for allowing us to illustrate the method with the "Sud-Ouest" Project data.

References

[1] Cardot, H., Faivre, R. and Goulard, M. (2003). Functional approaches for predicting land use with the temporal evolution of coarse resolution remote sensing data. *J. of Applied Statistics*, **30**, 1185-1999.

[2] Cardot, H., Faivre, R. and Maisongrande, P. (2004). Random Effects Varying Time Regression Models: Application to Remote Sensing. *Compstat 2004 proceedings* ed. J. Antoch, Physica-Verlag, 777-784.

[3] Coret L., P. Maisongrande, A.A. Boone, A. Lobo Aleu, G. Dedieu and P. Gouaux (2005). Documentation of the Drought impact with SPOT/HRVIR images tile Series over South-Western France. *International Journal of Remote Sensing*, **26**, 2461-2469.

[4] Déjean S., Faivre, R. and Goulard, M. (2002). Modèle non linéaire à paramètres aléatoires de la dynamique de cultures observées par télédétection : comparaison de deux procédures d'estimation. *J. Soc. Française De Statist.*, **143**, 205-213.

[5] Dierckx, P. (1993). *Curve and Surface Fitting with Splines.* Clarendon Press, Oxford.

[6] Diggle, P. J., Liang, K-Y. and Scott, S. L. (1994). *Analysis of longitudinal data.* Oxford University Press.

[7] Duchemin, B., and Ph. Maisongrande (2002). Normalisation of directional effects in 10-day global syntheses derived from VEGETATION/SPOT. I Investigation of concepts based on simulation. *Remote Sensing of Environment*, **81**, 90-100.

[8] Ducrot, D, Gouaux, P. (2004). Caractérisation des agro-systèmes de la plaine alluviale de la Garonne et des coteaux du Gers, mise en évidence de leurs changements au cours des dix dernires années. *Colloque Société Française Economie Rurale, Systèmes de production: performances, évolution, perspectives*, Lille.

[9] Faivre, R. and Fischer A., (1997). Predicting crop reflectances using satellite data observing mixed pixels. *Journal of Agricultural, Biological and Environmental Statistics*, **2**, 87-107.

[10] Foody, G.M. and Cox, D.P. (1994). Sub-pixel land cover composition estimation using a linear mixture model and fuzzy membership functions. *International Journal of Remote Sensing*, **15**, 619-631.

[11] Hastie, T. and Tibshirani, R. (1990). *Generalized Additive Models.* London, Chapman & Hall.

[12] Hoover, D.R., Rice, J.A., Wu, C.O. and Yang, L.P. (1998). Nonparametric smoothing estimates of time-varying coefficient models with longitudinal data. *Biometrika*, **85**, 809-822.

[13] Laird, N. and Ware, J. (1982). Random-Effects Models for Longitudinal Data. *Biometrics*, **38**, 963-974.

[14] McLachlan, G. and Krishnan, T. (1997). *The EM Algorithm and Extensions.* John Wiley & Sons.

[15] Maisongrande, P., B. Duchemin, G. Dedieu, (2004). VEGETATION/SPOT - An Operational Mission for the Earth Monitoring : Presentation of New Standard Products. *International Journal of Remote Sensing*, **25**, 9-14.

[16] Moulin, S., Bondeau, A., and R. Delécolle (1998). Combining agricultural crop models satellite observations : from field to regional scales. *International Journal of Remote Sensing*, **19**, 1021-1036.

[17] Moulin S., Fischer A. , Dedieu G. and R. Delécolle (1995). Temporal variations in satellite reflectances at field and regional scales compared with values simulated by linking crop growth and SAIL models. *Remote Sensing of Environment*, **54**, 261-272.

[18] Kastens J.H., Kastens T.L, Kastens D.L.A., Price K.P, Martinko E.A and Re-Yang Lee (2005). Image masking for crop yield forecasting using AVHRR NDVI time series imagery. *Remote Sensing of Environment*, **99**, 341-356.

[19] Knipling E.B. (1970). Physical and physiological basis for the reflectance of visible and near-infrared radiation from vegetation. *Remote Sensing of Environment*, **3**, 155-159.

[20] Lobell, D.B. and G. P. Asner (2004). Cropland distributions from temporal unmixing of MODIS data. *Remote Sensing of Environment*, **93**, 412-422.

[21] Ramsay, J., Silverman, B.W. (2005). *Functional Data Analysis.* Springer-Verlag, 2nd ed..

[22] Rice, J. (2004). Functional and longitudinal data analysis: Perspectives on smoothing. *Statistica Sinica*, **14**, 631-647.

[23] Rice, J. and Wu, C. (2001). Nonparametric mixed effects models for unequally sampled noisy curves. *Biometrics*, **57**, 253-259.

[24] Richards J.A., Jia, X. (2005). *Remote Sensing Digital Image Analysis: An Introduction.* Springer-Verlag, Berlin, 4th ed..

[25] Richardson A.J. and Wiegang, C.L., (1977). Distinguishing Vegetation from Soil Background Information. *Photogrammetric Engineering and Remote Sensing*, **43**, 1541-1552.

[26] Ridao, E., Conde J.R and M.I. Mnguez (1998). Estimating fAPAR from Nine Vegetation Indices for Irrigated and Nonirrigated Faba Bean and Semileafless Pea Canopies. *Remote Sensing of Environment*, **66**, 87-100.

[27] Robinson, G.K. (1991). That BLUP is a good thing: The estimation of random effects. *Statistical Science*, **6**, 15-51.

[28] Tucker, C.J., (1979). Red and Photographic Infrared Linear Combinations for Monitoring Vegetation. *Remote Sensing of Environment*, **8**, 127-150.

[29] Wikle, C., Millif, R., Nychka, D. and L. Berliner. (2001). Spatiotemporal Hierarchical Bayesian Modeling: Tropical Ocean Surface Winds. *J. of the American Statistical Association*, **96**, 382-397.

[30] Wooldridge, J. (2002). *Econometric Analysis of Cross Section and Panel Data.* Cambridge, MA, MIT Press.

[31] Wu, H., and Liang, H. (2004). Backfitting Random Varying-Coefficient Models with Time-Dependent Smoothing Covariates. *Scand. J. of Statist.*, **31**, 3-19.